Adv. Radio Sci., 11, 31–36, 2013
www.adv-radio-sci.net/11/31/2013/
doi:10.5194/ars-11-31-2013

Advances in Radio Science

Electromagnetic diffraction and scattering of a complex-source beam by a semi-infinite circular cone

H. Brüns and L. Klinkenbusch

Institut für Elektrotechnik und Informationstechnik, Christian-Albrechts-Universität zu Kiel, Germany

Correspondence to: L. Klinkenbusch (lbk@tf.uni-kiel.de)

Abstract. A complex-source beam (CSB) is used to investigate the electromagnetic scattering and diffraction by the tip of a perfectly conducting semi-infinite circular cone. The boundary value problem is defined by assigning a complex-valued source coordinate in the spherical-multipole expansion of the field due to a Hertzian dipole in the presence of the PEC circular cone. Since the incident CSB field can be interpreted as a localized plane wave illuminating the tip, the classical exact tip scattering problem can be analysed by an eigenfunction expansion without having the convergence problems in case of a full plane wave incident field. The numerical evaluation includes corresponding near- and far-fields.

1 Introduction

Scattering and diffraction of a plane electromagnetic wave by a semi-infinite perfectly electrically conducting (PEC) circular cone has often been treated in the literature. A survey on this subject can be found in the classical monograph by (Bowman et al., 1987). More recently, the scattered field has been obtained by a multipole-based integration of the exact surface-currents for the case of an incident plane wave. However, that solution suffers from a missing convergence of the finally obtained multipole series, and the application of suitable series-transformation techniques has been necessary to asymptotically derive the corresponding limiting values (Klinkenbusch, 2007; Kijowski and Klinkenbusch, 2011). Particularly, we are interested in the fields related the cone's apex, as the corresponding scattered field can act as a further element to complete asymptotic methods like the Geometrical Theory of Diffraction (GTD) and the Uniform Theory of Diffraction (UTD).

For the analysis of the influence of the tip on the scattered field, we have used a localized plane wave, that is, a complex-source beam (CSB) as the incident field. This can be achieved by simply assigning a complex-valued location to a dipole source. The width, focus length, and direction of incidence of the CSB can be controlled nearly arbitrarily (Orlov and Peschel, 2010). Combining this powerful tool with the spherical-multipole expansion provides a convergent eigenfunction solution with focusses on the evaluation of the scattered related to the tip of the cone.

Section 2 summarizes the solution of Maxwell's equations in the presence of a PEC circular cone, and in Sect. 3 the complex-source technique is introduced. Finally, we present some numerical results in Sect. 4.

2 Solution of Maxwell's equations in the presence of a PEC semi-infinite circular cone

Consider a perfectly electrically conducting (PEC) circular cone as illustrated in Fig. 1 with a half outer opening angle ϑ_0 embedded in a homogeneous medium with permittivity ε and permeability μ. We are looking for a solution of the time-harmonic Maxwell's equations at a time factor $e^{+j\omega t}$.

2.1 Helmholtz equation in spherical coordinates

The homogenous scalar Helmholtz equation

$$\Delta\Phi(r,\vartheta,\varphi) + \kappa^2\Phi(r,\vartheta,\varphi) = 0 \tag{1}$$

with the wave number $\kappa = \omega\sqrt{\varepsilon\mu}$ can be solved in spherical coordinates r, ϑ, φ (ϑ represents the polar coordinate.) by a classical separation ansatz. We finally obtain the following elementary solution

$$\Phi_\nu^m(r,\vartheta,\varphi) = z_\nu(\kappa r)Y_\nu^m(\vartheta,\varphi) \tag{2}$$

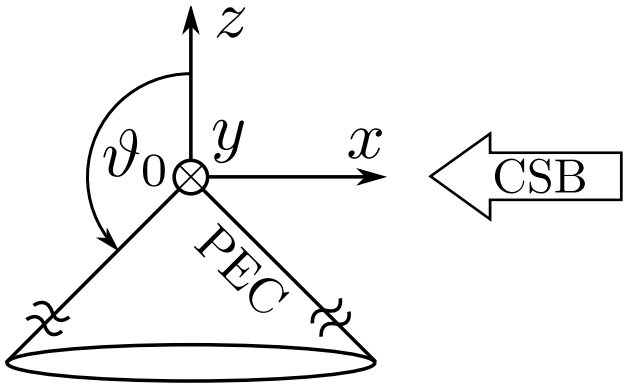

Fig. 1. A PEC, semiinfinite, circular cone located on the negative z-axis. The half outer opening angle is ϑ_0. A CSB incides from x-direction.

with z_ν being spherical Bessel functions related to (ordinary) Bessel functions by

$$z_\nu(\kappa r) = \sqrt{\frac{\pi}{2\kappa r}} Z_{\nu+1/2}(\kappa r) \tag{3}$$

Particularly we will need (everywhere regular) spherical Bessel functions of the first kind, $j_\nu(\kappa r)$, and spherical Hankel functions of the second kind, $h_\nu^{(2)}(\kappa r)$, satisfying the radiation condition at the chosen time factor $e^{+j\omega t}$.

The spherical harmonics $Y_\nu^m(\vartheta,\varphi)$ are defined as

$$Y_\nu^m(\vartheta,\varphi) = N_\nu^m P_\nu^m(\cos\vartheta) e^{jm\varphi}, \tag{4}$$

that is, as products of associated Legendre functions of the first kind $P_\nu^m(\cos\vartheta)$ in ϑ, and harmonic functions in φ. The normalization constant N_ν^m is chosen such that

$$\int_0^{\vartheta_0}\int_0^{2\pi} \left|Y_\nu^m(\vartheta,\varphi)\right|^2 \sin\vartheta \, d\vartheta d\varphi = 1. \tag{5}$$

2.2 Determination of eigenvalues

For the given geometry the solution has to be 2π-periodic in φ, hence the eigenvalues m have to be integral. In order to get solutions of the Helmholtz equation for a PEC circular cone as depicted in Fig. 1, these solutions have to fulfill the boundary conditions on the cone's surface. Therefore we need spherical harmonics that satisfy the Dirichlet condition as well as spherical harmonics that satisfy the Neumann condition at $\vartheta = \vartheta_0$. This can be achieved by finding eigenvalues ν_d and ν_n (Blume and Krebs, 1994) according to the transcendental equations

$$P_{\nu_d}^m(cos\ \vartheta)|_{\vartheta_0} = 0 \tag{6}$$

$$\left.\frac{\partial P_{\nu_n}^m(cos\ \vartheta)}{\partial\vartheta}\right|_{\vartheta_0} = 0 \tag{7}$$

which have been solved by means of a suitable numerical procedure, e.g. a bisection method.

Moreover, it has been shown by (Katsav et al., 2012) that for all valid eigenvalue pairs (ν, m) it holds that

$$m^2 \le \nu(\nu+1). \tag{8}$$

Figure 2 shows the eigenvalue pairs for $\vartheta_0 = 135°$ and $\nu_{\max} = 40$ in the ν, m-plane.

2.3 Spherical-multipole expansion

Within a homogeneous domain, any solution of Maxwell's equations outside the sources can be constructed by means of a complete set of spherical-multipole functions defined by

$$\boldsymbol{M}(\boldsymbol{r}) = (\boldsymbol{r}\times\nabla)\,\Phi(\boldsymbol{r}) \tag{9}$$

$$\boldsymbol{N}(\boldsymbol{r}) = \left(\frac{1}{\kappa}\nabla\times(\boldsymbol{r}\times\nabla)\right)\Phi(\boldsymbol{r}) \tag{10}$$

provided that Φ is a solution of the scalar homogeneous Helmholtz Eq. (1). They are determined according to

$$\boldsymbol{M}_{\nu,m}(r,\vartheta,\varphi) = z_\nu(\kappa r)\ \boldsymbol{m}_{\nu,m}(\vartheta,\varphi) \tag{11}$$

$$\begin{aligned}\boldsymbol{N}_{\nu,m}(r,\vartheta,\varphi) = &-\frac{z_\nu(\kappa r)}{\kappa r}\ \nu(\nu+1)Y_{\nu,m}(\vartheta,\varphi)\boldsymbol{e_r}\\ &-\frac{1}{\kappa r}\frac{d}{dr}[r z_\nu(\kappa r)]\boldsymbol{n}_{\nu,m}(\vartheta,\varphi)\end{aligned} \tag{12}$$

where $\boldsymbol{m}$ and $\boldsymbol{n}$ denote the transvere multipole functions:

$$\begin{aligned}\boldsymbol{m}_{\nu,m}(\vartheta,\varphi) = &-\frac{1}{\sin\vartheta}\frac{\partial Y_{\nu,m}(\vartheta,\varphi)}{\partial\varphi}\boldsymbol{e}_{\vartheta}\\ &+\frac{\partial Y_{\nu,m}(\vartheta,\varphi)}{\partial\vartheta}\boldsymbol{e}_{\varphi}\end{aligned} \tag{13}$$

$$\begin{aligned}\boldsymbol{n}_{\nu,m}(\vartheta,\varphi) = &\frac{\partial Y_{\nu,m}(\vartheta,\varphi)}{\partial\vartheta}\boldsymbol{e}_{\vartheta}\\ &+\frac{1}{\sin\vartheta}\frac{\partial Y_{\nu,m}(\vartheta,\varphi)}{\partial\varphi}\boldsymbol{e}_{\varphi}.\end{aligned} \tag{14}$$

To accomplish that the tangential part of the electric field vanishes on the PEC cone's surface, the spherical-multipole expansion of the total field reads

$$\boldsymbol{E}(\boldsymbol{r}) = \sum_{\nu_d,m} a_{\nu_d,m}^{II(I)}\boldsymbol{N}_{\nu_d,m}^{II(I)}(\boldsymbol{r}) + \frac{Z}{j}\sum_{\nu_n,m} b_{\nu_n,m}^{II(I)}\boldsymbol{M}_{\nu_n,m}^{II(I)}(\boldsymbol{r}) \tag{15}$$

and for the magnetic field

$$\boldsymbol{H}(\boldsymbol{r}) = \frac{j}{Z}\sum_{\nu_d,m} a_{\nu_d,m}^{II(I)}\boldsymbol{M}_{\nu_d,m}^{II(I)}(\boldsymbol{r}) + \sum_{\nu_n,m} b_{\nu_n,m}^{II(I)}\boldsymbol{N}_{\nu_n,m}^{II(I)}(\boldsymbol{r}). \tag{16}$$

$$r > r',\ (r < r') \tag{17}$$

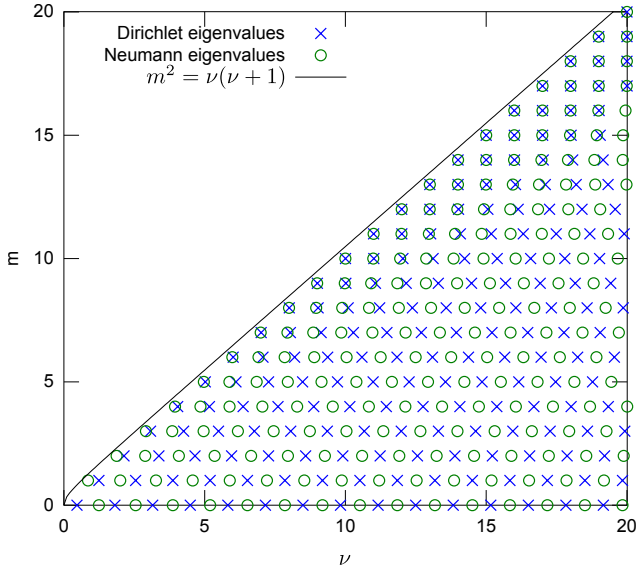

Fig. 2. Pairs of eigenvalues for $\vartheta_0 = 135°$, $\nu_{\max} = 20$.

where ν_d and ν_n are eigenvalues of the Dirichlet and Neumann type, respectively. $Z = \sqrt{\mu/\varepsilon}$ represents the intrinsic wave impedance of the homogeneous domain. The indices (I) and (II) stand for the use of spherical Bessel functions j_ν or spherical Hankel functions of the second kind $h_\nu^{(2)}$ are used according to Eq. (17) (see also Sect. 4). The multipole amplitudes $a_{\nu_d,m}$ and $b_{\nu_d,m}$ can be determined for a Hertzian dipole source at $\boldsymbol{r}'$ electrically polarized in $\boldsymbol{c_e}$ according to

$$a_{\nu_d,m}^{II(I)} = -\kappa_0^2 Z_0 \frac{(-1)^m}{\nu_d(\nu_d+1)} \boldsymbol{N}_{\nu_d,-m}^{I(II)}(\boldsymbol{r}') \cdot \boldsymbol{c_e}\,, \tag{18}$$

$$b_{\nu_n,m}^{II(I)} = -j\kappa_0^2 \frac{(-1)^m}{\nu_n(\nu_n+1)} \boldsymbol{M}_{\nu_n,-m}^{I(II)}(\boldsymbol{r}') \cdot \boldsymbol{c_e}\,. \tag{19}$$

The electric far-field is found from the asymptotic form of the spherical Hankel function of the second kind for large arguments as

$$\boldsymbol{E}_\infty(\boldsymbol{r}) = \left(\frac{e^{-j\kappa r}}{\kappa r}\right)\left[\sum_{\nu_d,m} -j^{\nu_d} a_{\nu_d,m}^{II} \boldsymbol{n}_{\nu_d,m} + \frac{Z}{j}\sum_{\nu_n,m} j^{(\nu_n+1)} b_{\nu_n,m}^{II} \boldsymbol{m}_{\nu_n,m}\right]. \tag{20}$$

For the evaluation of the scattered field, we simply need to subtract the incident field from the total field where the incident field is computed by a similar approach using a free space spherical-multipole expansion.

3 Complex-source beam

The complex-source beam (CSB) offers the possibility to describe a focussed beam analytically. If a complex valued location is assigned to a dipole source, a Gaussian beam is generated. The beam's focus, width, and direction can be controlled arbitrarily by the chosen complex location. The complex location vector of the source has the form

$$\boldsymbol{r}_c' = \boldsymbol{r}_r' - j\boldsymbol{r}_i'\,, \tag{21}$$

where $\boldsymbol{r}_r'$ gives the actual position of the beam's waist and $\boldsymbol{r}_i'$ the direction of incidence. The absolute value of $\boldsymbol{r}_i'$ correspond to the rayleigh length of the generated Gaussian beam. To clarify this, we insert a complex $\boldsymbol{r}'$ into the free space Green's function. We choose a purely imaginary location $\boldsymbol{r}'$:

$$\boldsymbol{r}\,' = -jz_0\boldsymbol{e}_z\,. \tag{22}$$

That means, the beam has a rayleigh length z_0, has it's waist in the origin, and propagates in z-direction. Assuming a small distance $\rho = \sqrt{x^2+y^2}$ from the z-axis, a second order taylor series expansion of $|\boldsymbol{r}-\boldsymbol{r}'|$ delivers a paraxial approximation:

$$|\boldsymbol{r}-\boldsymbol{r}\,'| = \sqrt{x^2+y^2+(z+jz_0)^2} \tag{23}$$
$$\approx \left((z+jz_0) + \frac{1}{2}\frac{\rho^2}{(z+jz_0)}\right), \quad \rho \ll z, \quad z > 0$$

Inserting Eq. (23) into the Green's function we get:

$$G(\boldsymbol{r},\boldsymbol{r}\,') = \frac{1}{4\pi}\frac{e^{-j\kappa|\boldsymbol{r}-\boldsymbol{r}'|}}{|\boldsymbol{r}-\boldsymbol{r}\,'|} \tag{24}$$
$$\approx \frac{1}{4\pi(z+jz_0)}\exp\left(-j\kappa(z+jz_0) - \frac{j\kappa\rho^2}{2(z+jz_0)}\right)$$
$$= \frac{\exp(\kappa z_0)}{4\pi(z+jz_0)}\exp\left(-j\kappa z - \frac{j\kappa\rho^2}{2\left(z+\frac{z_0^2}{z}\right)} - \frac{\rho^2}{\frac{2z_0}{\kappa}\left(1+\frac{z_0^2}{z^2}\right)}\right).$$

Ignoring the factor $\exp(\kappa z_0)/4\pi(z+jz_0)$, the result of Eq. (24) directly correspond to the form of the Gaussian beam:

$$\exp(-j\kappa z)\exp\left(-\frac{j\kappa\rho^2}{2R(z)}\right)\exp\left(-\frac{\rho^2}{w^2(z)}\right). \tag{25}$$

By comparing Eqs. (24) and (25) we can identify following beam parameters: The radius of curvature R is

$$R(z) = z + \frac{z_0^2}{z}\,. \tag{26}$$

The radius w of the beam is

$$w(z) = w_0\sqrt{1+\left(\frac{z}{z_0}\right)^2}, \tag{27}$$

where w_0 is the radius at the waist:

$$w_0 = \sqrt{\frac{2z_0}{\kappa}}. \tag{28}$$

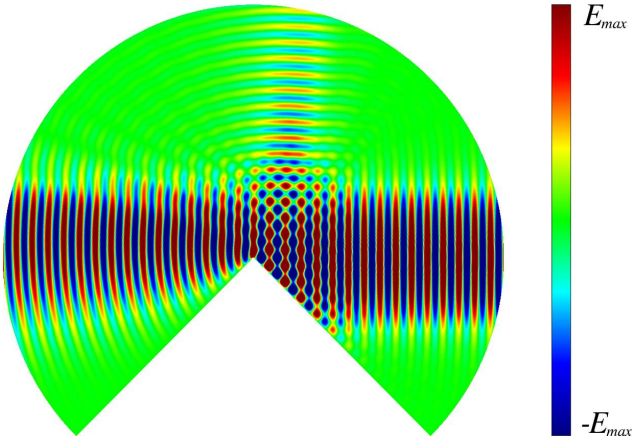

Fig. 3. E_y in the x,z-plane.

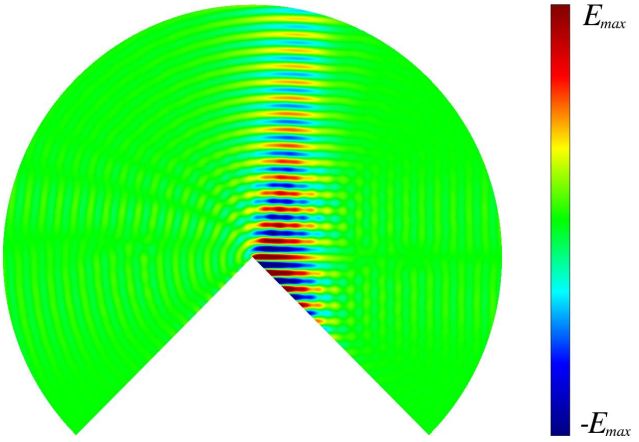

Fig. 4. H_x in the x,z-plane within a range of $r \leq 20$m.

As we can see in Eq. (26), the radius of curvature gets large for $z \ll z_0$. That means that there are nearly plane wave fronts close to the beam's waist which are – due to the transverse Gaussian profile – also localized.

4 Treatment of a complex-valued coordinate in the spherical-multipole expansion

The following equations are special cases of the Gegenbauer addition theorem applied to spherical Bessel functions of zeroth order

$$\frac{\sin(\kappa R)}{\kappa R} = \sum_{n=0}^{\infty} (2n+1)\, j_n(\kappa r)\, j_n(\kappa r')\, P_n(\cos\gamma), \tag{29}$$

$$-\frac{\cos(\kappa R)}{\kappa R} = \sum_{n=0}^{\infty} (2n+1)\, j_n(\kappa r)\, y_n(\kappa r')\, P_n(\cos\gamma). \tag{30}$$

They are valid for arbitrary complex r, r', γ, κ and provided that

$$|r e^{\pm j\gamma}| < |r'| \tag{31}$$

and

$$R = \sqrt{r^2 + r'^2 - 2rr'\cos\gamma}. \tag{32}$$

Having two position vectors $\boldsymbol{r}(r,\vartheta,\varphi)$ and $\boldsymbol{r}'(r'\vartheta',\varphi')$, the distance $|\boldsymbol{r}-\boldsymbol{r}'|$ between this positions can be expressed by R if we choose

$$\cos\gamma = \cos\vartheta\cos\vartheta' + \sin\vartheta\sin\vartheta'\cos(\varphi-\varphi'). \tag{33}$$

By combining Eqs. (29), (30) and the relation

$$P_n(\cos\gamma) = \frac{4\pi}{2n+1} \sum_{m=-n}^{+n} Y_n^m(\vartheta,\varphi) Y_n^{m*}(\vartheta',\varphi') \tag{34}$$

we can construct a spherical multipole expansion of the scalar free space Green's function:

$$g(\boldsymbol{r},\boldsymbol{r}') = \frac{1}{4\pi}\frac{e^{-j\kappa|\boldsymbol{r}-\boldsymbol{r}'|}}{|\boldsymbol{r}-\boldsymbol{r}'|} \tag{35}$$

$$= \sum_{n=0}^{\infty}\sum_{m=-n}^{+n} j_n(\kappa r) h_n^{(2)}(\kappa r') Y_n^m(\vartheta,\varphi) Y_n^{m*}(\vartheta',\varphi').$$

This expansion is valid for any complex location $\boldsymbol{r}'$, if the condition Eq. (31) is fulfilled. If it is not, $\boldsymbol{r}$ and $\boldsymbol{r}'$ can be permuted due to the Green's function symmetry. This paper only deals with CSBs that point directly to the tip of the cone, so there is only a complex r'-component (Katsav et al., 2012). In this case γ is real and the condition that has to be fulfilled is

$$|r| < |r'|. \tag{36}$$

This must be considered for the multipole expansions in section 2.3, particulary for Eq. (17), if a complex-source beam is used.

5 Numerical results

The following results are for a circular cone with a half opening angle of 45° ($\vartheta_0 = 135°$) and are calculated with multipole expansions according to the preceding sections using a maximum order $\nu_{\max} = 40$. The coordinates of the CSB are $r' = (12 + j48)$ m, $\vartheta' = 90°$, $\varphi' = 0°$; this means that the beam has a rayleigh length of 48 m and propagates from x-direction to the tip of the cone. The electric field of the beam is polarized in y-direction. The wave number is $\kappa = 5$/m. Figure 3 shows the y-component of the electric field in a x,z-crosscut through the cone. The beam is partly reflected and and there is interference between the incident and the reflected field. Above the beam's part that has passed the tip we can observe less strong interference with scattered parts

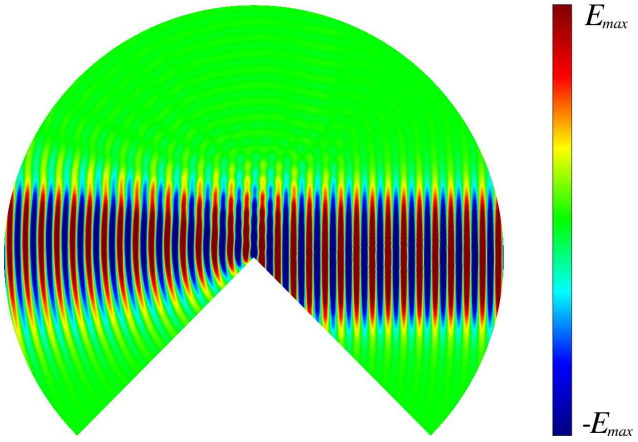

Fig. 5. H_z in the x, z-plane within $r \leq 20$m.

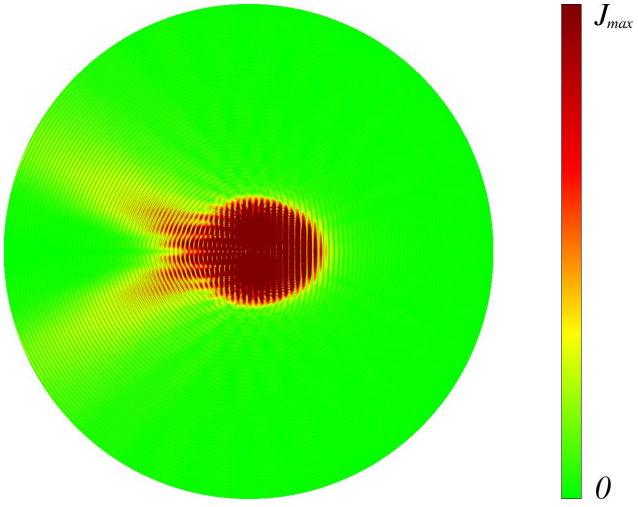

Fig. 6. Current density distribution on the cone's surface in the region $r \leq 40$m. View from z-direction. The beam incides from right-hand side.

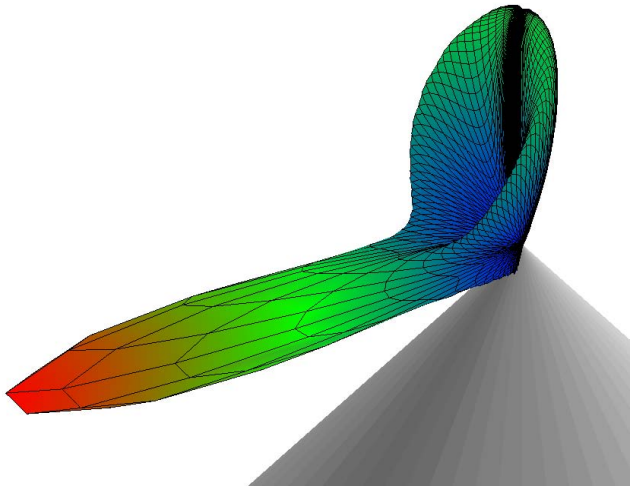

Fig. 7. Far-field pattern with the magnitude of the electric field.

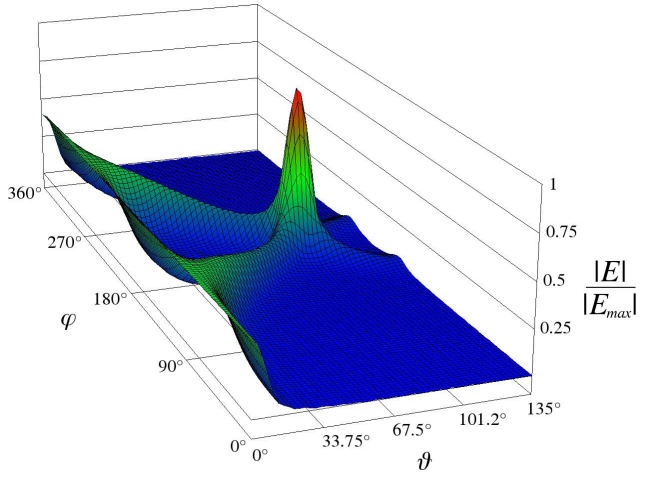

Fig. 8. Magnitude of the electric far-field plotted against ϑ, φ.

of the beam. In the shadow region of the cone we can clearly see diffracted spherically shaped wavefronts. Figure 4 and 5 show the x- and the z-component of the magnetic field. While the incident part of the magnetic field is polarized in z-direction, the reflected part is polarized in x. In both figures diffracted parts can be found. Figure 6 shows the current density distribution on the cone's surface, which can be calculated with

$$\boldsymbol{J}_s(\boldsymbol{r}) = -\boldsymbol{e}_\vartheta \times \boldsymbol{H}(\boldsymbol{r})|_{\vartheta=\vartheta_0}\,. \tag{37}$$

There are two notable creeping waves in the shadow region of the cone. Finally, the magnitude of the scattered far-field is examined; in Fig. 7 it is shown in the form of a far-field pattern, in Fig. 8 it is plotted against ϑ, φ. The beam is reflected in every direction of φ; the highest values are observed in the direction of propagation. For $90° < \vartheta < 135°$ we observe two relatively small maxima, particulary in Fig. 8. This might be a consequence of the creeping waves, which can be observed in Fig. 6 of the current density.

6 Conclusions

The scattering of an electromagnetic CSB by a semi-infinite circular cone has been analysed using spherical multipole expansions. Convergent results of the total or scattered field can be obtained for both near- and far-field. So far, only beams pointing directly to the tip of the cone have been considered. Future work will expand this approach to other geometries, e.g. elliptic cones. Furthermore the requirements for CSBs pointing in arbitrary directions will be investigated, so that other parts of the cone can be illuminated.

Acknowledgements. This work was supported by the Deutsche Forschungsgemeinschaft (KL815/10-1&2).

References

Bowman, J. J., Senior, T. B. A., and Uslenghi, P. L. E., Electromagnetic and acoustic scattering by simple shapes (Revised Printing), Hemisphere Pub. Corp., New York, 1987.

Blume, S. and Krebs, V.: Der Rückstreuquerschnitt des semiinfiniten Kreiskegels, Arch. Elektrotech., 77, 239–244, 1994

Katsav, M., Heyman, E., and Klinkenbusch, L.: Complex-source beam diffraction by an acoustically soft or hard circular cone, Electromagnetics in Advanced Applications (ICEAA), 2012 International Conference on, proceedings, Cape Town, South Africa, 2–7 September 2012, 135–138, 2012

Kijowski, M. and Klinkenbusch, L.: Eigenmode analysis of the electromagnetic field scattered by an elliptic cone, Adv. Radio Sci., 9, 31–71, 2011

Klinkenbusch, L.: Electromagnetic scattering by semi-infinite circular and elliptic cones, Radio Sci., 42, RS6S10, doi:10.1029/2007RS003649, 2007

Orlov, L. and Peschel, U.: Complex source beam: A tool to describe highly focused vector beams analytically, Phys. Rev. A, 82, 063820, doi:10.1103/PhysRevA.82.063820, 2010